Large enhancements of $NaYF_4$:Yb/Er/Gd nanorod upconversion emissions via coupling with localized surface plasmon of Au film

2014 Nanotechnology 25 185401

(http://iopscience.iop.org/0957-4484/25/18/185401)

IOP Publishing Nanotechnology
Nanotechnology **25** (2014) 185401 (9pp) doi:10.1088/0957-4484/25/18/185401

Large enhancements of $NaYF_4$:Yb/Er/Gd nanorod upconversion emissions via coupling with localized surface plasmon of Au film

Qi Luo[1], Yanrui Chen[1], Zhiqiang Li[1], Feng Zhu[1], Xiaohong Chen[1], Zhuo Sun[1], Yunle Wei[2], Hai Guo[2], Zeng Bo Wang[3] and Sumei Huang[1]

[1] Engineering Research Center for Nanophotonics and Advanced Instrument, Ministry of Education, Department of Physics, East China Normal University, North Zhongshan Rd. 3663, Shanghai 200062, People's Republic of China
[2] Department of Physics, Zhejiang Normal University, Jinhua, Zhejiang 321004, People's Republic of China
[3] School of Electronic Engineering, Bangor University, Dean Street, Bangor, Gwynedd, LL57 1UT, UK

E-mail: smhuang@phy.ecnu.edu.cn

Received 4 November 2013, revised 24 February 2014
Accepted for publication 11 March 2014
Published 15 April 2014

Abstract

Four-layered plasmonic structures of glass/Au/TiO_2/$NaYF_4$:Yb, Er, Gd nanorods were fabricated and tremendous improvement in upconversion luminescence (UCL) was observed under infrared 980 nm excitation. The TiO_2 film was used as an oxide spacer. The emission intensity of the upconversion (UC) nanorods was strongly modulated by the thickness of the TiO_2 layer. The extent of modulation depended on the separation distance between the Au layer and UC nanorods. A maximum UCL enhancement of 192-fold was observed for one green emission (540 nm) when a 10 nm-thick TiO_2 film was used; 150-fold was observed for the other green emission (521 nm) at the same thickness of TiO_2; and 105-fold was observed for the red emission (654 nm) when a 7.5 nm-thick TiO_2 film was used. Alteration of the radiative decay rate was demonstrated for the first time in measurements of the decay times of UC nanorods positioned at various distances from the Au layer. The light interaction and coupling between metal Au and UC nanorods is numerically studied. The UCL mechanisms of multilayer plasmonic structures are discussed. Experimental results are explained and correspond well with those of theoretical calculations.

Keywords: plasmon enhancement, upconversion, lanthanide-doped nanomateria, fluorophore–metal interaction, thin film silicon solar cell

(Some figures may appear in colour only in the online journal)

1. Introduction

Upconversion (UC) emission nano-materials can convert low frequency excitation photons into high frequency emission photons through two-photon or multi-photon processes [1, 2]. Various kinds of UC materials have been developed for different applications such as three dimensional displays [3], spectral converters for solar cells [4, 5] and biolabels [6]. Recently, new, simple and quick synthesis routines have been reported to form lanthanide-doped nanometer-sized crystals in

order to share the high efficiencies of their bulk equivalents [5, 7, 8]. As a result, lanthanide-doped UC nanoparticles have attracted much attention [9]. However, UC nanoparticles generally have smaller photoluminescence (PL) efficiency than their bulk counterparts due to the small absorption cross sections arising from formally forbidden f-level atomic transitions of the dopants and the existence of a variety of quenchers in their large surface area [10], prompting a need for methods of enhancing their luminescence.

The use of plasmonic nanostructures based on rare earth ion doped UC nanocrystals and noble metals such as Au or Ag nanoparticles (NPs) is currently a very active research field for fluorescence signal amplification. Schietinger *et al* observed a UC emission enhancement from a single $NaYF_4$:Yb^{3+}/Er^{3+} nanocrystal coupled with gold spheres by use of a combined confocal atomic force microscope [8]. An overall enhancement factor of 3.8 was achieved by this system. Zhang *et al* showed that an enhancement factor of approximately 2.6 can be achieved by attaching $NaYF_4$:Yb^{3+}/Tm^{3+} nanocrystals to gold NPs [11]. We also studied the UC luminescence (UCL) properties of $NaYF_4$:Yb^{3+}/-Er^{3+}/-Gd^{+3} nanocrystals coupled with Au NP or nanoshells in our previous work [5]. Beyond direct coating with an Au or Ag nanoshell or sphere, indirect coating with an inert SiO_2 shell and then the Au or Ag nanoshell [11–13], Au island films [14] and patterned Au surfaces [15] have also demonstrated the feasibility of enhancement of UC emissions through plasmon interactions. In a core–shell structure of $NaYF_4$:Yb,Er@SiO_2@Ag reported by Yuan *et al* [13], the separation distance between Ag and the UC NPs was demonstrated to be of vital importance for the extent of the enhancement effect, and the maximum enhancement factor was 14.4. Very recently, Saboktakin *et al* [16] reported a configuration in which close-packed monolayers of UC NPs are separated from a layer of nanoimprint patterned metal NPs (Au or Ag) by a nanometer-scale noble metal-oxide (Al_2O_3) grown by atomic layer deposition. Luminescence enhancements were found to be dependent on the thickness of the oxide spacer layer and the type of metal NP with enhancements of up to 5.2-fold proximal to Au NPs and of up to 45-fold proximal to Ag NPs.

Since rare-earth doped NPs have variations in size, shape, defect density, doping concentration, luminescence quantum efficiency, etc, and metal nanostructures also have variations in size and shape, their inhomogeneity makes detailed discussion of the mechanism of UCL enhancement very difficult. Although the potential of metallic nanostructures for amplification of UC emission efficiency in UC nanomaterials has been demonstrated, the process of their fabrication remains difficult. It is also hard to obtain consistent enhancements. The reported results widely differ in the factors of fluorescence enhancement, from fractional (quenching) to large amplification of more than 100-fold [17]. This is largely due to small changes in the particles' plasmonic features that result from minute variations in the size, shape, composition, environment, and geometry of the composites used in the study. Therefore, fabrication of metallic nanostructures or a robust nanofabrication procedure with reproducible plasmonic properties is one of the important aspects of metal-enhanced fluorescence.

In this paper, we describe a simple method for the fabrication of a four-layered plasmonic structure of glass-noble metal-transition metal-oxide (TiO_2)-UC nanorods that displays up to 192-fold fluorescence enhancement. The reported method mainly employs a simple vacuum deposition process. First, we synthesized pure hexagonal-phase Yb^{3+}-Er^{3+}-Gd^{+3} codoped sodium yttrium fluoride ($NaYF_4$:Yb/Er/Gd) nanorods by a liquid–solid–solution process. Second, we deposited 50 nm-thick Au layers on glass substrates by direct current (DC) sputtering. Third, we deposited TiO_2 layers on the sputtered Au films by radio frequency (RF) sputtering, tuned the deposition thickness of TiO_2, and fabricated multilayered plasmonic structures using the grown $NaYF_4$:Yb/Er/Gd nanorods. The performances of the formed plasmonic structures were evaluated over a broad spectral range from UV to NIR wavelength range. We show that the UC fluorescence can be modulated through adjusting the thickness of the TiO_2 layer. The light interaction and coupling between the metal Au nanofilm and UC nanorods was numerically studied. From the correlation between the UCL enhancement factors and local field intensities at UC emissions as well as the UCL enhancement and the change of the fluorescence lifetime, we discuss the mechanism of the PL enhancement.

2. Experimental details

$NaYF_4$: Yb, Er, Gd nanorods were synthesized according to the procedures described in Refs. [5, 7]. Briefly, a deionized water solution (7.5 ml) of 1.5 g NaOH was mixed with 25 ml of ethanol and 25 ml of oleic acid under stirring. 10 ml of $RECl_3$ (0.2 M, RE = Y, Yb, Er, and Gd, YCl_3:$YbCl_3$:$ErCl_3$:$GdCl_3$ = 50:18:2:30 mol%) solution and 5 ml of NH_4F (2 M) was added to the resulting mixture. Then the solution was transferred into a 100 mL Teflon-lined autoclave and heated to 200 °C for 2 h to obtain the nanorods. The nanorods were washed with ethanol and water several times and collected by centrifugation. Finally, the nanorods were re-dispersed into ethanol to form an aqueous dispersion and ready for use.

Gold films with a thickness of 50 nm were deposited on cleaned glass substrates using DC sputtering at a rate of 2.6 Å s^{-1}. TiO_2 layers with various thicknesses from 0 to 25 nm were deposited onto the prepared Au films by RF sputtering from a titanium dioxide ceramic target at a rate of 0.25 Å s^{-1}. Then, the as-deposited UC nanorods were spin-coated onto the sputtered TiO_2 films to form multilayered plasmonic samples for the following characterization and analysis.

Multilayered plasmonic Au/TiO_2/$NaYF_4$:Yb, Er, Gd samples were examined and characterized. The morphology was examined by field emission scanning electron microscopy (SEM). Fluorescence spectra were recorded on a HORIBA Jobin Yvon fluoromax-4 fluorescence spectrophotometer equipped with a commercial near-infrared laser (CW 980 nm). The excitation laser is incident on the front layer of multilayered plasmonic samples at an angle of about 45° from the normal line. The emission light is collected at the same side of the sample. The 45° excitation was performed because the near-infrared laser light was more

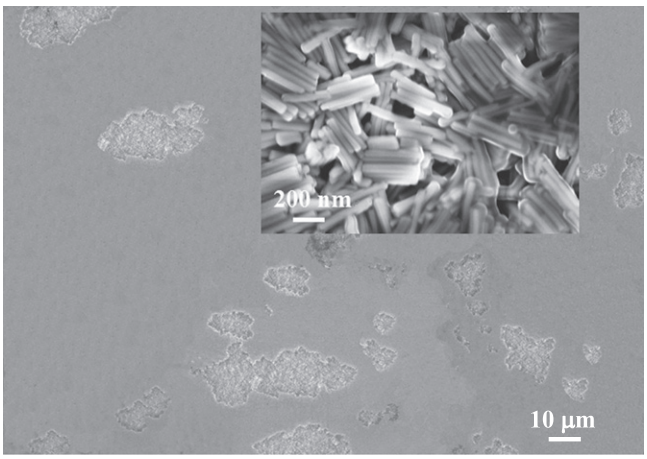

Figure 1. SEM image of spin-coated $NaYF_4$: Yb, Er, Gd nanorod film.

conveniently introduced at oblique incidence during UC emission measurement. Time-resolved spectra and UC PL lifetime measurements were performed on a SBP500 monochromator (Zolix Instruments, Beijing, China) coupled to a Hamamatsu R928 photomultiplier (Hamamatsu, Japan) with Tektronix TDS5052 oscilloscope (Tektronix Inc., Beaverton, OR) and a nanosecond pulsed 980-nm laser as the excitation source [18]. This excitation laser is also incident on the plasmonic sample at an angle of about 45°. All the measurements were carried out at room temperature. UV-vis spectra were taken by a Hitachi U-3900 UV-Vis spectrophotometer.

3. Result and discussion

In the prepared plasmonic Au/TiO_2/$NaYF_4$:Yb, Er, Gd samples, both the deposited Au and TiO_2 films are very smooth and featureless. The smooth TiO_2 layer was employed to control the spacing distance between the Au and $NaYF_4$: Yb, Er, Gd nanorod films. Figure 1 shows a SEM image of a spin-coated $NaYF_4$: Yb, Er, Gd nanorod layer. The image exhibits a random and tenuous appearance characteristically observed for colloidal aggregates or fractals. In the nanorod aggregated areas, one or two/three layers of UC nanorods were formed with partial ordering, as demonstrated in the inset of figure 1. At the region near the aggregated areas, some sparse nanorods presented. The as-prepared UC nanorods have a hexagonal structure with a uniform size of 70–80 nm in diameter and approximately 300–500 nm in length [5].

The UC emission properties of the formed plasmonic structures are TiO_2 layer thickness-dependent. Figure 2(a) shows UC emission spectra of the samples with TiO_2 layers of different thicknesses. The thickness of the TiO_2 spacer increased from 0 nm to 25 nm by a step of 2.5 nm, and a sample with UC nanorods on glass without Au/TiO_2 was used as a reference. The emission spectra were collected under CW 980 nm laser excitation. The excitation laser is incident on the front side of the sample at an angle of 45° and with a power of

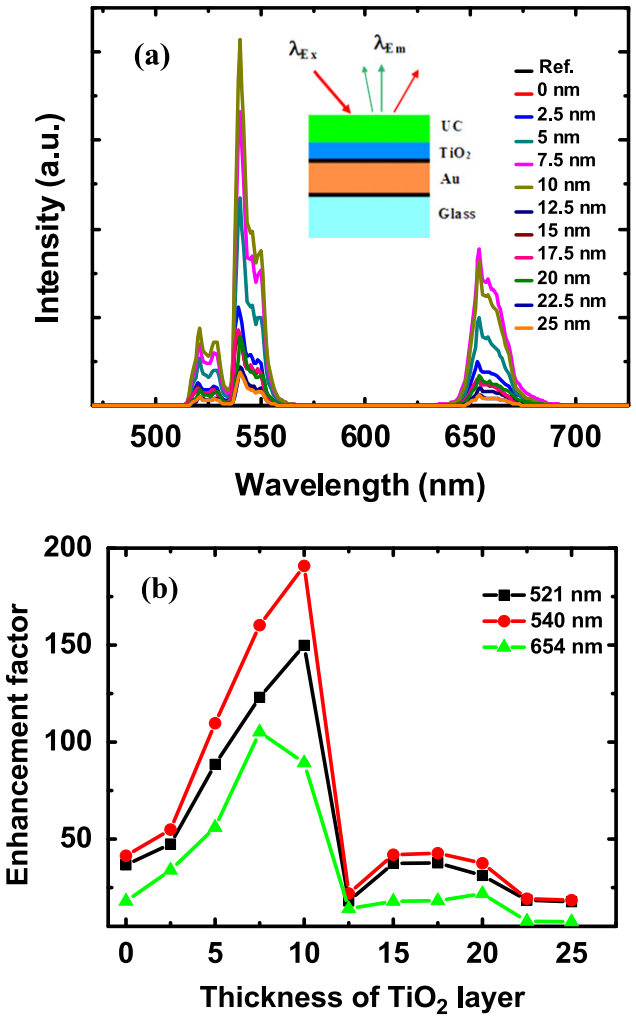

Figure 2. (a) UC emission spectra of plasmonic samples with TiO_2 layers of different thicknesses, (b) UCL enhancement factor as a function of TiO_2 layer thickness.

300 mW as demonstrated in the inset of figure 2(a). The measured UC spectrum exhibits two strong emission bands at 540 and 654 nm, and a weak emission peak at 521 nm, corresponding to $^4S_{3/2} \rightarrow {}^4I_{15/2}$, $^4F_{9/2} \rightarrow {}^4I_{15/2}$ and $^2H_{11/2} \rightarrow {}^4I_{15/2}$ transitions of Er^{3+}, respectively [19–21]. We plot the intensities of these three groups of bands (which are defined as the integral over the band spectral region) as functions of the TiO_2 spacer layer thickness, and find that the enhancement factor of the UC signal is strongly related to the TiO_2 thickness, as depicted in figure 2(b). Compared with the case of the bare $NaYF_4$:Yb/Er/Gd nanorods on glass, the enhancement factors of the two green peaks at 520–550 nm and the red band at 654 nm are 37, 42 and 18, respectively, for the sample with the bare Au film, i.e., without a spacer (0 nm-thick TiO_2 layer). Both green bands (521 and 540 nm) increase synchronously and continuously in emission intensity with the thickness of the TiO_2 layer increasing from 0 nm to 10 nm, reach maximal enhancement factors of 150 and 192 at 10 nm-thick TiO_2, respectively, and then exhibit a quicker decrease when the thickness of the TiO_2 layer increases further. The luminescence intensity of the red (654 nm) band shows a

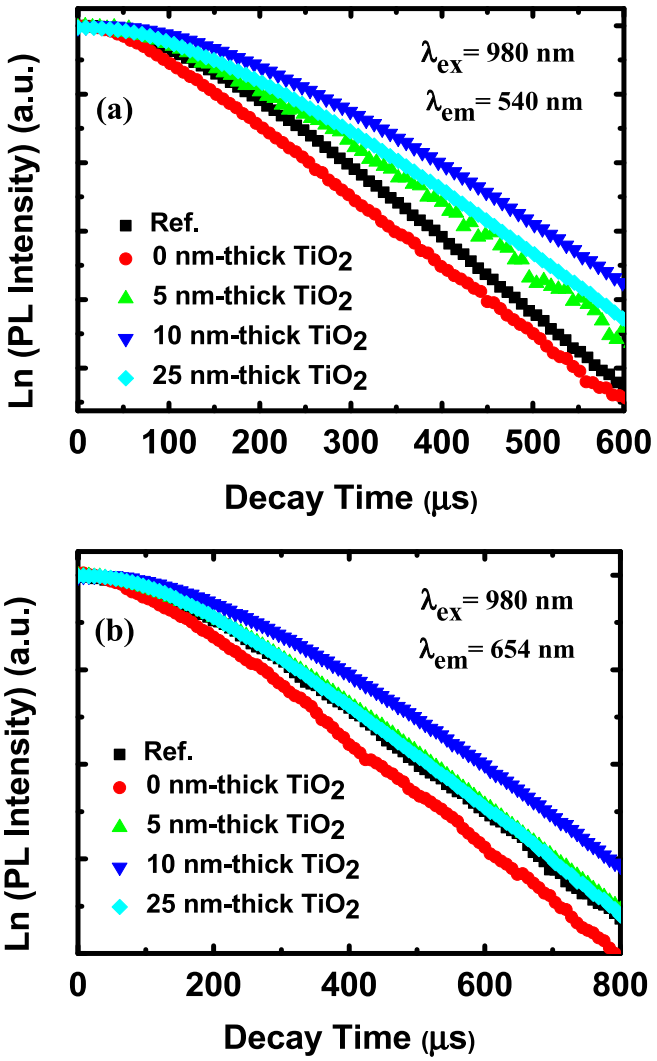

Figure 3. Luminescence decay curves of Er^{3+} in plasmonic samples with TiO_2 layers of different thicknesses. (a) Decay time at 540 nm, (b) decay time at 654 nm.

quite similar trend with the increase of the titanium dioxide thickness, but its maximum UCL enhancement value of 105 is reached at 7 nm-thick TiO_2, as shown in figure 2(b). Moreover, a preferential enhancement of the green emission band across the range of TiO_2 spacers was demonstrated.

Surface plasmons (SPs) are in general described as oscillating electronic excitations near a metal surface and can be well determined by classical electrodynamics [22–25]. Additionally, the excited fluorophore induces a charge distribution on the metal surface. If this plasmon can radiate then the fluorophore emission is observed as plasmon-coupled emission. If the induced plasmon cannot radiate then the fluorophore appears to be quenched. The fluorophore–metal interactions are still described by classical electrodynamics. The origin of the plasmonic UC enhancement effect on rare-earth doped nanocrystals from noble metal nanostructures or surfaces is attributed to two possible reasons in previous papers: (1) an increase in the effective excitation induced by local field enhancement; or (2) the increase in both non-radiative and radiative decay rates of fluorophores and the

Table 1. Decay times τ_{decay} of green (540 nm) and red (654 nm) UC emission from plasmonic samples with TiO_2 layers of different thicknesses.

Sample	τ_{decay} (540 nm)	τ_{decay} (654 nm)
Ref.	293 μs	519 μs
0 nm-thick TiO_2	276 μs	425 μs
5 nm-thick TiO_2	313 μs	531 μs
10 nm-thick TiO_2	328 μs	577 μs
25 nm-thick TiO_2	311 μs	522 μs

consequent degeneration of fluorescence decays and decrease in fluorescence lifetimes due to the optical frequency of the UC emission in near resonance with the surface plasmon frequency of noble metals known as surface plasmon coupled emission (SPCE) [8, 11, 22, 26]. Based on experimental phenomena, other explanations have also been proposed. For example, Feng *et al* ascribed the effective luminescence enhancement from Ag islands and sub-micron Ag nanowires attached $NaYF_4$: Yb, Er NCs to the size induced different scattering efficiency [27]. Zhang *et al* considered the local crystal field changes as a possible route to enhancing UC in cubic $NaYF_4$ NPs covered with Au shells [11].

To verify how Au NPs enhance the UC of nanorods further, we measured time-resolved spectra and UC PL lifetimes for four-layered plasmonic samples under a pulse at 980 nm. Figure 3 shows the luminescence decay curves of Er^{3+} in the plasmonic samples with different TiO_2 thicknesses. The time-resolved spectrum from the sample with the bare Au film without oxide spacer is significantly different to that from glass. The decay times of the green and red UC emission from the samples with TiO_2 layers of different thicknesses are shown in table 1. As shown in table 1, the decay times τ_{decay} of green (540 nm) and red (654 nm) UC emission from the reference are 293 μs and 519 μs, respectively. UC nanorods directly assembled on the Au nanofilm surface exhibit obviously shorter decay times (276 μs at 540 nm and 425 μs at 654 nm) compared with the corresponding reference sample. In contrast, compared to the reference sample, the decay times of Er^{3+} UC emission levels of plasmonic samples with TiO_2 layers were all prolonged, as shown in figures 3(a) and (b). With the increase of TiO_2 thickness from zero, the τ_{decay} values of the green and the red emissions increased, reached maximum 328 μs and 557 μs, respectively, when the TiO_2 thickness was 10 nm, and then decreased when the TiO_2 thickness further increased from 10 nm to 25 nm. The prolonged decay time is evidently not in agreement with the character of the previous reported resonance fluorescence enhancement or SCPE for UC nanocrystals, in which the coupling of UC emissions with surface plasmon resonance in metal nanostructures will lead to increased radiative decay rates, that is, shortening lifetimes [5, 8, 11, 22, 26]. However, our results are in good agreement with the early and classic reports about the effects of metallic surfaces on fluorescence from molecular systems [28–30]. In these reports, altering the radiative decay rate was observed in measurements of the decay times of europium (Eu^{3+})

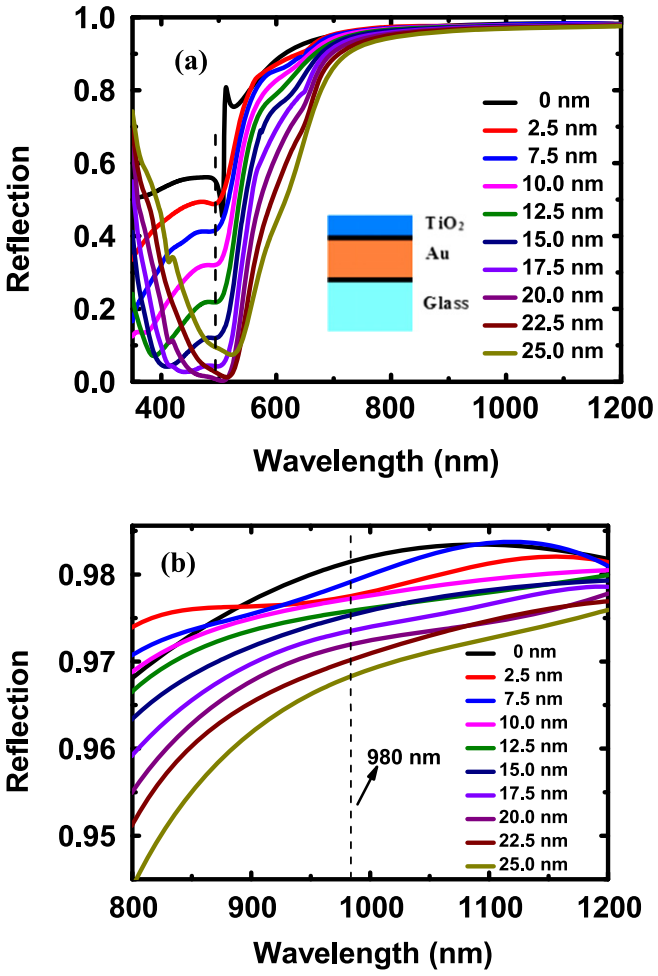

Figure 4. Calculated reflection spectra of glass/50 nm-thick Au/0–25 nm thick TiO_2 structures. The wave is incident at a 45° angle from the normal on the front layer of the sample. (a) Reflection spectra in 380 nm–1200 nm, (b) reflection spectra in 800–1200 nm.

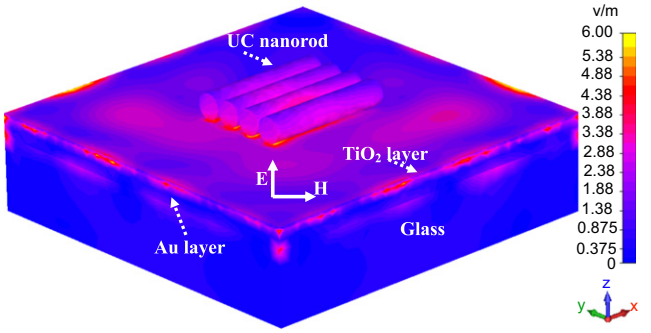

Figure 5. 3D electric field amplitude |*E*| enhancement distribution for a transverse electromagnetic wave at 654 nm wavelength with 45° angle incident on a four-layered plasmonic structure with a 10 nm-thick TiO_2.

positioned at various distances from a planar metal mirror using Langmuir-Blodgett films. The data also showed a dramatic decrease in lifetime when the europium complex is within 10 nm of the metal surface. This decrease is interpreted as being due to lossy surface waves (LSWs) which quench the fluorophore at short distances. The lifetimes oscillate with distance from the mirror. The oscillations in lifetime can be quantitatively explained by the reflected far-field radiation from the fluorophore back on itself, which is called the reflective model [31].

In order to deeply explain the TiO_2 thickness-dependent luminescence enhancement shown in figure 2, we carried out a simulation considering a broadband plane wave as the illumination source for the sample with different TiO_2 thicknesses (L). The wavelength-dependent dielectric constant used in the calculations, $\varepsilon(\lambda) = \varepsilon'(\lambda) + i\varepsilon''(\lambda)$, was directly taken from the bulk experimental data in Palik's book [32]. A commercial FIT (finite integral technique) software package (CST Microwave Studio 2011) was used with a Cartesian grids system (FDTD (finite difference time domain) module) [33]. The wave is incident at a 45° angle from air on the front layer of the sample as demonstrated in the inset of figure 4(a). The calculated reflection spectra of three layer, glass /Au/0–25 nm thick TiO_2 structures are shown in figure 4. While the dips in the reflection spectra can be expected to correspond to the resonances [34, 35], their position is observed to shift towards longer wavelengths in the 490–530 nm range as shown in figure 4(a). The dip position is red-shifted from 490 nm (with 2.5 nm TiO_2 layer) to 521 nm (with 25 nm TiO_2 layer). Therefore, deep dips, which clearly move in accordance with L, were regarded as signs of resonance. The plasmon red-shift occurs due to the presence of the TiO_2 layer because of the higher refractive index of TiO_2 relative to vacuum. The thicker TiO_2 layer covering the Au film may also screen the electron oscillation in the metal, decreasing the plasmon energy [36]. Moreover, the glass /Au/TiO_2 structure with thin TiO_2 layer shows a high reflection in the 600–1050 nm spectral range. In particular, when L is 0–10 nm, the structure has a reflectance of over 97.5% at the pumping laser (980 nm), but when L increases from 10 nm, its reflection at 980 nm presents a continuous decrease from about 97.5% to 96.5%. The reflection property shows a very similar TiO_2 thickness dependence, especially in the L range of 10 nm to 25 nm, as does the UCL shown in figure 3. Except when the UC nanorods are close to the metal, the significant UC PL enhancement at 7.5–10 nm thick TiO_2 coincides nicely with the high reflection property in 520–980 nm range shown in figures 4(a) and (b).

The light scattering and coupling in the actual experimental samples, four layer, glass-Au-TiO_2-UC nanorod plasmonic systems, was also numerically studied based on a three-dimensional (3D) model. The dielectric constant of UC nanorods is taken as 1.55[2]. The electric field distribution was also solved with CST Microwave Studio 2011, with periodic boundary conditions in the lateral directions, perfect match layers in the normal direction, and a plane wave incident on the front layer of the sample at an angle of 45° as the excitation source, as shown in figure 5. The incident wave is linearly polarized. The electric vector makes an angle of 45° with the x-coordinate (the UC nanorod). We investigated the local electric field enhancement created by the four-layered plasmonic samples. Figure 5 shows the calculated local amplitude enhancement distribution of the electric field, |*E*|,

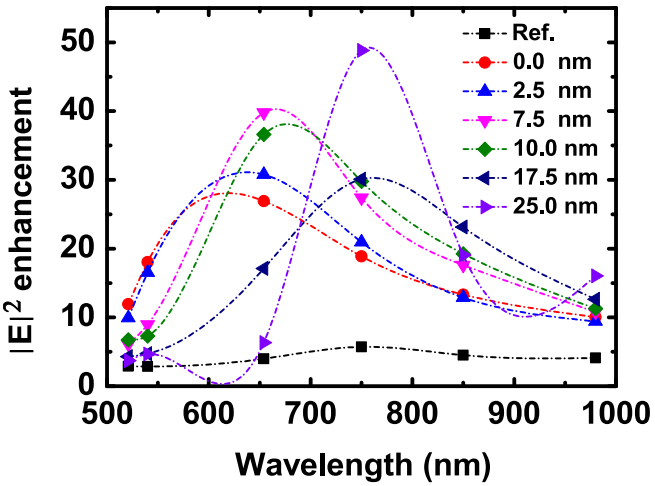

Figure 6. Maximal local electric field intensity $|E|^2$ enhancement within the four UC nanorods as a function of wavelength. The smoothing spline fit is included as a guide to the eye.

for an incident wave with a wavelength of 654 nm for the sample with a 10 nm-thick TiO_2. The electric fields are strongly localized and enhanced in the Au layer-UC nanorod gaps due to the multi-scattering, constructive interference and strong coupling between them. The maximal electric field $|E|$ enhancement at 645 nm is over 6 for this sample with a 10 nm-thick TiO_2. We plot the maximal local electric field intensity $|E|^2$ enhancement within the four UC nanorods as the function of wavelength in figure 6. It clearly shows that the field intensity $|E|^2$ enhancement is very low for the reference sample without Au layer, while with the application of Au layer, the $|E|^2$ enhancement values obviously increase over the 521–980 nm wavelength range. The field intensity enhancement at both UC green emission peaks (521 nm and 540 nm) decreases with the increase of TiO_2 thickness from 0 nm to 25 nm as expected, however, the $|E|^2$ enhancement reaches its maximum of 39-fold at 654 nm for 7.5 nm-thick TiO_2 and then, 49-fold at 750 nm for 25 nm-thick TiO_2. The maximal $|E|^2$ enhancement at 654 nm for the 7.5 nm-thick TiO_2 sample can explain its highest UCL enhancement of the red emission shown in figure 2. Moreover, following the smoothing spline fit shown in figure 6, the field intensity $|E|^2$ enhancement peak is red-shifted from 616 nm (with 0 nm TiO_2 layer) to 759 nm (with 25 nm TiO_2 layer). The result can be associated with the red-shift of plasmon resonance shown in figure 4. When TiO_2 L is 7.5 nm, the $|E|^2$ enhancement peak is at 660 nm, close to the frequency of the red emission (654 nm). Therefore, the maximal UCL enhancement for the red emission shown in figure 2(b) is attributed to the frequency matching between the plasmon resonance of the multilayer plasmonic sample and the red emission of UC nanorods.

The UC emission mechanism of Er^{3+} has already been well documented in the literature [19–21, 37]. Its visible emissions are produced through multiple processes including ground-state absorption (GSA), excited-state absorption (ESA) and energy transfer (ET). In our Yb^{3+}/Er^{3+} codoped $NaYF_4$ samples, for the green emission, a Yb^{3+} ion is excited by a 980 nm photon from the ground state ($^2F_{7/2}$) to the excited state ($^2F_{5/2}$) through the GSA process, and then transfers the energy to an Er^{3+} ion and promotes it from $^4I_{15/2}$ to $^4I_{11/2}$. At the same time, the populated $^4I_{11/2}$ level is excited to the $^4F_{7/2}$ state by ESA of a second photon. The populated $^4F_{7/2}$ then relaxes rapidly and nonradiatively to the next lower $^2H_{11/2}$ and $^4S_{3/2}$ levels due to the small energy gap between them. The radiative transition from the $^2H_{11/2}$, $^4S_{3/2}$ to the $^4I_{15/2}$ level process emits green at 521 nm and 540 nm, respectively. The red emission in the Yb^{3+}/Er^{3+} codoped $NaYF_4$ system is a bit more complex since the ESA, ET and cross-relaxation (CR) processes are all involved. When the $^4I_{11/2}$ level is excited by ET from Yb^{3+}, part of the $^4I_{11/2}$ level relaxes nonradiatively to the $^4I_{13/2}$ level. Three transition processes as follows: ET: $^4I_{13/2}$ (Er) + $^2F_{5/2}$ (Yb) → $^4F_{9/2}$ (Er) + $^2F_{7/2}$ (Yb), ESA: $^4I_{13/2}$ (Er) + hν → $^4F_{9/2}$ (Er), and CR: $^4I_{13/2}$ (Er) + $^4I_{11/2}$ (Er) → $^4F_{9/2}$ (Er) + $^4I_{15/2}$ (Er), contribute greatly to populating the $^4F_{9/2}$ level. The energy transfer process is particularly dominant stemming from the high concentration of Yb^{3+} ions and the large absorption cross section of the $^2F_{7/2} - {}^2F_{5/2}$ transition of Yb^{3+} compared to that of the $^4I_{15/2} - {}^4I_{11/2}$ transition of Er^{3+}. The radiative transition from the $^4F_{9/2}$ to the $^4I_{15/2}$ level process emits red light at 654 nm.

In addition to the plasmonic UC enhancement mechanisms (LEF and SPCE) described in the previous section, there are other mechanisms influencing the absorption and emission of different types of fluorophores. In particular, these are the photoinduced electron transfer and Förster Resonance Energy Transfer (FRET) that are favored by short distances between the metal nanostructures and fluorescence emitters. Both effects can lead to efficient fluorescence quenching. In essence, wave-vector matching [38] for each explicit plasmon-fluorophore event determines whether a photon will be emitted to far-field or be quenched [26]. Normally, at a few-nanometer distance, the metal is prone to quench the fluorescence, while at intermediate distances (approximately 5–50 nm) fluorophore emission is dominating, with an optimum typically in the 10–20 nm range; exact distances are physically dependent on the specific materials, geometry, and nanoscale systems [8, 11–13, 22, 26, 38]. For planar metal surfaces, fluorophore-to-metal distances of about 10–100 nm enhance the fluorescence by SPCE. Fluorescence quenching by LSWs becomes completely dominating below about 10 nm [22]. A cubed quenching distance (d^3) dependence by LSWs has been shown [39]. In our planar plasmonic structures, the distance-dependent UCL enhancement or quenching results shown in figure 2 consist well with previous reports [11–13, 22, 26, 38, 39].

From UCL lifetime measurements in figure 3, the plasmonic sample with the bare Au layer exhibits shorter decay times (276 μs at 540 nm and 425 μs at 654 nm) compared with the corresponding reference sample. This decay time shortening for UP emissions is consistent with previous studies on rare-earth doped nanocrystals [5, 8, 11–16], suggesting that both green (41-fold) and red (18-fold) UC enhancements of the bare Au sample originate from the increased emission rates. For the plasmonic sample with the bare Au layer, and the UC nanorods assembled at the lowest level directly in

contact with the Au layer, quenching (electron transfer and FRET) becomes completely dominating. However, since UC nanorods have a diameter of 70 nm, the nanorods at top levels are situated too far away to be quenched, and thus, 18–41-fold UCL enhancements are obtained. For the plasmonic sample with a TiO_2 layer as a spacer, application of the TiO_2 layer changes the micro-environments around the UC nanorods. As the TiO_2 thickness increases from 0 nm to 25 nm, energy transfer processes slow down more compared to those in direct contact, and the local field intensity enhancement at both green emissions (521 nm and 540 nm) keeps decreasing; however, the $|E|^2$ enhancement at longer wavelengths evolves in a different way. As the TiO_2 thickness increases from 0 to 25 nm, the $|E|^2$ enhancement for a wavelength of 654 nm first increases, reaches a maximum (39-fold) at 7.5-nm thick TiO_2, keeps a very high value (37-fold) at 10 nm-thick TiO_2, and then decreases very quickly. The maximal $|E|^2$ enhancement at 654 nm results in the largest PL red enhancement (105-fold) from a 7.5 nm-thick TiO_2 sample due to the strong coupling of the UC red emission with the plasmonic resonance of the Au layer. Although $|E|^2$ enhancements at both green emission peaks for 7.5 nm-thick TiO_2 are a little higher than those for 10 nm-thick TiO_2, the maximal UC PL enhancements at these two green bands occur at the latter, probably due to the relatively stronger quenching effect with the former. Moreover, the sample with a 25 nm-thick TiO_2 has the largest field intensity $|E|^2$ enhancement at the pumping laser (980 nm), as shown in figure 6, but it has the very small green and red luminescence enhancements shown in figures 2(a) and (b). Additionally, the significant UC green and red luminescence enhancement at 7.5–10 nm thick TiO_2 shown in figure 2 coincides nicely with the high reflection property in the 520–980 nm range from the Au layer shown in figure 4, and also agrees well with the high local field intensity $|E|^2$ enhancement from constructive interference and strong coupling between SPs of Au surface and emissions of UC nanorods shown in figure 6. These results suggest that the TiO_2 thickness dependent luminescence enhancement might be associated with changes in the reflected field from the Au layer with distance, the effects of the reflected field on the fluorophores,and that the enormous green (150-fold at 521 nm and 192-fold at 540 nm) and red (107-fold) luminescence enhancements are attributed to the strong coupling between the Au layer and UC nanorods. Due to plasmon-emitter decoupling between the UC nanorod emissions and metal Au SPs in the sample with the thicker (>10 nm) TiO_2, luminescence enhancement decreases considerably as shown in figures 2(a) and (b).

From the UCL lifetime measurements shown in figure 3 and table 1, with the increase of TiO_2 thickness from zero, the τ_{decay} values of the green and red emissions first increased, reached maxima at 10 nm thick TiO_2, and then decreased when the TiO_2 thickness increased from 10 nm to 25 nm. In the early report about a Eu^{3+} complex in front of a silver mirror [30], three oscillations in lifetime at various distances of 1–100 nm, 100–300 nm and 300–500 nm were observed. This phenomenon is quantitatively explained by considering the radiation field from an excited molecule S, given by the Hertz classical equation. The field arrives at the molecule, after being reflected at the mirror (an acceptor A), with a retardation effect [31]. Moreover, an excited state population can decay by LSWs, transfer to surface plasmons or decay to far-field radiation. Theoretical calculation based on electrodynamic theory shows that radiative decay dominates above 100 nm, transfer to surface plasmons occurs from 10 to 400 nm, and quenching by LSWs is the dominant process below 10 nm for the Eu^{3+} complex-metal system [22, 40]. In our system, the energy transfer from the excited UC nanrod to the metal Au can be treated in a similar manner by considering the phenomenon as a retardation effect. From the fluorophore–metal interaction calculation in the actual experimental samples shown in figure 6, when the TiO_2 thickness is thin (2.5–10 nm), the enormous local field intensities will change the micro-environments around UC nanorods, influence the GSA of Yb^{3+} and the ESA of Er^{3+}, promote the UC populating processes and consequently increase PL. From figure 3, comparing with the reference sample, the plasmonic sample with TiO_2 has longer decay times (311–328 μs at 545 nm and 522–557 μs at 654 nm) in their temporal evolution curves of Er^{3+}, which possibly means that more energy has been transferred from excited Yb^{3+} ions to Er^{3+} ions to enhance UC populating processes of Er^{3+} ions in these Au and TiO_2 modified samples. The more efficient UC ET, ESA or CR processes keep the $^4S_{3/2}$ or $^4F_{9/2}$ (Er) levels at higher populations. The higher population at these levels is favorable for the radiative transition from the $^4S_{3/2}$ to the $^4I_{15/2}$ level process by emitting green at 540 nm, or from the $^4F_{9/2}$ to the $^4I_{15/2}$ level process by emitting red light at 654 nm. Consequently, the 10 nm-thick TiO_2 sample with the longest decay times shows the first strongest UCL enhancement at green emissions and the second strongest UCL enhancement at red emission. Liu *et al* have studied the UC properties of Au@β-NaYF4:Yb,Tm nanocrystals [17]. They also reported that attaching Au nanoparticles on UC nanocrystals lengthened the lifetimes of both Yb^{3+} and Tm^{3+} excited states and resulted in the enhanced UC emissions of Tm^{3+}.

In this work, the fabricated multilayer plasmonic structures of glass/Au/TiO_2/$NaYF_4$:Yb, Er, Gd nanorods offered tremendous UC emission enhancements in both green and red bands under the NIR light. Therefore, they can be expected to be applied to solar cell and new display technologies. In particular, the reported plasmonic structure can be used as a separate material component for thin film solar cells to allow an increase in the efficiency of the photo-conversion process in the infrared region, a range notoriously poor for the current commercial thin film solar cells [4, 5, 41]. We initially examined the feasibility of the prepared plasmonic samples for use in thin film solar cells. The fabricated plasmonic sample (glass/Au/10 nm-thick TiO_2/UC nanorods) was directly applied at the rear side of a planar thin film silicon solar cell [41]. The NIR laser is incident on the solar cell at an angle of about 45° from the normal line. The results have demonstrated that the UC of NIR light leads to a 60-fold enhancement of the photocurrent due to 980 nm illumination compared with a cell without the upconverter. This result

further confirmed the large UC emission enhancements in our multilayer plasmonic structures.

4. Conclusions

We have fabricated multilayer Au/TiO_2/$NaYF_4$:Yb, Er, Gd nanorod multilayer plasmonic structures for the first time and demonstrated considerable improvement in UCL owing to the effective coupling of UC nanorods with surface plasmons of Au nanometer film. Separation distance dependent UCL enhancement was investigated by controlling the thickness of the TiO_2 spacer. The emission intensity of the UC nanorods was found to be significantly modulated by the presence of the TiO_2 spacer. The extent of modulation was found to be strongly dependent on the separation distance between the Au layer and UC nanorods. The optimum UCL enhancements (105–192 times) were observed at a TiO_2 thickness of 10 nm for the green emissions and at a TiO_2 thickness of 7.5 nm for the red emission. Time-resolved spectra and PL lifetimes of the plasmonic structures were measured and analyzed. Alteration in the radiative decay rate was demonstrated in measurements of the decay times of erbium (Er^{3+}) positioned at various distances from the Au nanolayer. The light scattering and coupling in these multilayer plasmonic systems was numerically studied. Experimental results are explained and correspond quite well with those of theoretical calculations. An advantage of this approach lies in its ability to fabricate large area and steady optoelectronic devices with improved luminescence efficiency.

Acknowledgment

This work was supported by the National Natural Science Foundation of China (Nos. 11274119, 61275038).

References

[1] Wang X, Zhuang J, Peng Q and Li Y 2005 A general strategy for nanocrystal synthesis *Nature* **437** 121–4
[2] Wang F and Liu X 2009 Recent advances in the chemistry of lanthanide-doped upconversion nanocrystals *Chem. Soc. Rev.* **38** 976–89
[3] Downing E, Hesselink L, Ralston J and Macfarlane R 1996 A 3-color, solid-state, 3-dimensional display *Science* **273** 1185–9
[4] Shalav A, Richards B and Green M 2007 Luminescent layers for enhanced silicon solar cell performance: up-conversion *Sol. Energy Mater. Sol. Cells* **91** 829–42
[5] Li Z, Li X, Liu Q, Chen X, Sun Z, Liu C, Ye X and Huang S M 2012 Core/shell structured $NaYF_4$: Yb^{3+}/Er^{3+}/Gd^{+3} nanorods with Au nanoparticles or shells for flexible amorphous silicon solar cells *Nanotechnology* **23** 025402
[6] Abdul Jalil R and Zhang Y 2008 Biocompatibility of silica coated $NaYF_4$ upconversion fluorescent nanocrystals *Biomaterials* **29** 4122–8
[7] Wang F, Han Y, Lim C S, Lu Y, Wang J, Xu J, Chen H, Zhang C, Hong M and Liu X 2010 Simultaneous phase and size control of upconversion nanocrystals through lanthanide doping *Nature* **463** 1061–5
[8] Schietinger S, Aichele T, Wang H-Q, Nann T and Benson O 2010 Plasmon-enhanced upconversion in single $NaYF_4$: Yb^{3+}/Er^{3+} codoped nanocrystals *Nano Lett.* **10** 134–8
[9] Dong H, Sun L-D and Yan C-H 2013 Basic understanding of the lanthanide related upconversion emissions *Nanoscale* **5** 5703–14
[10] Boyer J-C and Van Veggel F C 2010 Absolute quantum yield measurements of colloidal $NaYF_4$: Er^{3+}, Yb^{3+} upconverting nanoparticles *Nanoscale* **2** 1417–9
[11] Zhang H, Li Y, Ivanov I A, Qu Y, Huang Y and Duan X 2010 Plasmonic modulation of the upconversion fluorescence in $NaYF_4$: Yb/Tm hexaplate nanocrystals using gold nanoparticles or nanoshells *Angew. Chem. Int. Edn.* **49** 2865–8
[12] Priyam A, Idris N M and Zhang Y 2012 Gold nanoshell coated NaYF4 nanoparticles for simultaneously enhanced upconversion fluorescence and darkfield imaging *J. Mater. Chem.* **22** 960–5
[13] Yuan P, Lee Y H, Gnanasammandhan M K, Guan Z, Zhang Y and Xu Q-H 2012 Plasmon enhanced upconversion luminescence of $NaYF_4$: Yb, Er@ SiO_2@ Ag core–shell nanocomposites for cell imaging *Nanoscale* **4** 5132–7
[14] Zhang H, Xu D, Huang Y and Duan X 2010 Highly spectral dependent enhancement of upconversion emission with sputtered gold island films *Chem. Commun.* **47** 979–81
[15] Paudel H P, Zhong L, Bayat K, Baroughi M F, Smith S, Lin C, Jiang C, Berry M T and May P S 2011 Enhancement of near-infrared-to-visible upconversion luminescence using engineered plasmonic gold surfaces *J. Phys. Chem.* C **115** 19028–36
[16] Saboktakin M, Ye X, Oh S J, Hong S-H, Fafarman A T, Chettiar U K, Engheta N, Murray C B and Kagan C R 2012 Metal-enhanced upconversion luminescence tunable through Metal nanoparticle–nanophosphor separation *ACS Nano* **6** 8758–66
[17] Liu N, Qin W, Qin G, Jiang T and Zhao D 2011 Highly plasmon-enhanced upconversion emissions from Au@ β-$NaYF_4$: Yb, Tm hybrid nanostructures *Chem. Commun.* **47** 7671–3
[18] Wei Y, Chi X, Liu X, Wei R and Guo H 2013 Novel upconversion behavior in Ho3+-doped transparent oxyfluoride glass-ceramics containing $NaYbF_4$ nanocrystals *J. Am. Ceramic Soc.* **96** 2073–6
[19] Pollnau M, Gamelin D R, Lüthi S R, Güdel H U and Hehlen M P 2000 Power dependence of upconversion luminescence in lanthanide and transition-metal-ion systems *Phys. Rev.* B **61** 3337–46
[20] Golding P, Jackson S, King T and Pollnau M 2000 Energy transfer processes in $Er3^+$-doped and $Er3^+$, $Pr3^+$-codoped ZBLAN glasses *Phys. Rev.* B **62** 856–64
[21] Auzel F 2004 Upconversion and anti-stokes processes with f and d ions in solids *Chem. Rev.* **104** 139–74
[22] Ford G and Weber W 1984 Electromagnetic interactions of molecules with metal surfaces *Phys. Reports* **113** 195–287
[23] Huang S, Hong M, Lukyanchuk B and Chong T 2003 Direct and subdiffraction-limit laser nanofabrication in silicon *Appl. Phys. Lett.* **82** 4809–11
[24] Wang Z, Luk'yanchuk B, Hong M, Lin Y and Chong T 2004 Energy flow around a small particle investigated by classical Mie theory *Phys. Rev.* B **70** 035418
[25] Wang Z, Guo W, Li L, Luk'yanchuk B, Khan A, Liu Z, Chen Z and Hong M 2011 Optical virtual imaging at 50 nm lateral resolution with a white-light nanoscope *Nature Commun.* **2** 218
[26] Hakonen A and Strömberg N 2011 Plasmonic nanoparticle interactions for high-performance imaging fluorosensors *Chemical Commun.* **47** 3433–5

[27] Feng W, Sun L-D and Yan C-H 2009 Ag nanowires enhanced upconversion emission of $NaYF_4$: Yb, Er nanocrystals via a direct assembly method *Chem. Commun.* 4393–5
[28] Drexhage K H 1974 IV Interaction of light with monomolecular dye lasers *Prog. Optics* **12** 161–232
[29] Amos R and Barnes W 1997 Modification of the spontaneous emission rate of $Eu3^+$ ions close to a thin metal mirror *Phys. Rev.* B **55** 7249–54
[30] Chance R, Miller A, Prock A and Silbey R 1975 Fluorescence and energy transfer near interfaces: the complete and quantitative description of the Eu/mirror systems *J. Chem. Phys.* **63** 1589–95
[31] Kuhn H 1970 Classical aspects of energy transfer in molecular systems *J. Chem. Phys.* **53** 101–8
[32] Palik E D 1985 *Handbook of Optical Constants of Solids* (Orlando, FL: Academic Press)
[33] Wang Z, Luk'yanchuk B, Guo W, Edwardson S, Whitehead D, Li L, Liu Z and Watkins K 2008 The influences of particle number on hot spots in strongly coupled metal nanoparticles chain *J. Chem. Phys.* **128** 094705
[34] Miyazaki H T and Kurokawa Y 2006 Controlled plasmon resonance in closed metal/insulator/metal nanocavities *Appl. Phys. Lett.* **89** 211126
[35] Pedrueza E, Valdés J L, Chirvony V, Abargues R, Hernández-Saz J, Herrera M, Molina S I and Martínez-Pastor J P 2011 Novel method of preparation of gold-nanoparticle-doped TiO_2 and SiO_2 plasmonic thin films: optical characterization and comparison with Maxwell–Garnett modeling *Adv. Funct. Mater.* **21** 3502–7
[36] Prodan E, Lee A and Nordlander P 2002 The effect of a dielectric core and embedding medium on the polarizability of metallic nanoshells *Chem. Phys. Lett.* **360** 325–32
[37] Suyver J, Aebischer A, García-Revilla S, Gerner P and Güdel H 2005 Anomalous power dependence of sensitized upconversion luminescence *Phys. Rev.* B **71** 125123
[38] Lakowicz J R, Ray K, Chowdhury M, Szmacinski H, Fu Y, Zhang J and Nowaczyk K 2008 Plasmon-controlled fluorescence: a new paradigm in fluorescence spectroscopy *Analyst* **133** 1308–46
[39] Campion A, Gallo A, Harris C, Robota H and Whitmore P 1980 Electronic energy transfer to metal surfaces: a test of classical image dipole theory at short distances *Chem. Phys. Lett.* **73** 447–50
[40] Lakowicz J R 2005 Radiative decay engineering 5: metal-enhanced fluorescence and plasmon emission *Anal. Biochem.* **337** 171–94
[41] Zhu H, Hüpkes J, Bunte E, Owen J and Huang S 2011 Novel etching method on high rate ZnO: Al thin films reactively sputtered from dual tube metallic targets for silicon-based solar cells *Sol. Energy Mater. Sol. Cells* **95** 964–8